

Photoacoustic measurement of thermal properties of TiN thin films

A. Albert Irudayaraj · R. Srinivasan · P. Kuppasami ·
E. Mohandas · S. Kalainathan · K. Ramachandran

Received: 4 July 2007 / Accepted: 23 October 2007 / Published online: 4 December 2007
© Springer Science+Business Media, LLC 2007

Abstract Titanium nitride (TiN) thin films were prepared by reactive DC magnetron sputtering under different nitrogen flow rates and at constant substrate temperature as well as at constant nitrogen flow rate and at different substrate temperatures. Photoacoustic measurement of the thermal properties of the films revealed that the thermal diffusivity and thermal conductivity of the TiN thin films are significantly lower than the bulk values and that the grain size of the films has substantial influence on the thermal properties of TiN thin films. The thermal conductivity of the films decreases with increasing nitrogen flow rates and increases with increasing substrate temperature. The above opposing behaviour in the thermal properties is found to be related to the microstructure, especially, the grain size of the films.

Introduction

Titanium nitride coatings have been widely applied as high temperature diffusion barrier for silicon devices in microelectronics, and wear resistant coatings in automobile industries [1–3]. These coatings are used as ohmic and Schottky contact layer in semiconductor devices [4, 5] and solar cells [6, 7], as gate electrodes and interconnections in very large-scale integration [8, 9], and as a replacement of polycrystalline silicon in very large-scale metal oxide semiconductor integrated circuits [10]. The other areas of applications include high temperature photothermal conversion [11], biomedical materials [12] and steel cutting tools [13].

Thermal property data are important for any material that experiences heat transfer. A knowledge of thermal diffusivity and thermal conductivity of TiN thin films is essential for their long-term use in devices and for understanding the thermal aging effects and deterioration of films in the area of microelectronics and tribology, where TiN films are used in one form or another. Techniques for thermal property measurements of thin films can be classified as contact [14–17] and non-contact methods [18, 19]. Contact methods are suitable only for dielectric thin films and the sample preparation process is tedious.

Photoacoustic (PA) method is a relatively new, simple, non-destructive and non-contact method for measuring thermal diffusivities of bulk materials as well as thin films [20]. It can be used to study opaque, transparent or highly scattering samples with minimal sample preparation and offers high sensitivity and precision over conventional methods [21]. In the PA method, a modulated light beam is irradiated on the sample contained in a sealed air-filled PA cell. The subsequent temperature fluctuation induced in the sample due to light absorption and non-radiative

A. Albert Irudayaraj
Department of Physics, Sacred Heart College, Tirupattur
635601, Tamil Nadu, India

R. Srinivasan
Department of Physics, Thiagarajar College, Madurai 625009,
Tamil Nadu, India

P. Kuppasami (✉) · E. Mohandas
Physical Metallurgy Division, Indira Gandhi Centre for Atomic
Research, Kalpakkam 603102, Tamil Nadu, India
e-mail: pk@igcar.gov.in

S. Kalainathan
Department of Physics, Vellore Institute of Technology, Vellore
632014, Tamil Nadu, India

K. Ramachandran
School of Physics, Madurai Kamaraj University, Madurai
625021, Tamil Nadu, India

de-excitation processes within the sample gives rise to thermal waves in the sample. The thermal waves propagate through the sample and on reaching the surface of the sample, they cause a modulated thermal expansion of the surrounding air, which can be detected by a microphone as acoustic signal. The amplitude of the PA signal depends on the heat generated in the sample and hence on the optical absorption coefficient and on the thermal properties of the sample [22]. The PA signal is largely dictated by the thermal diffusion length, μ [23],

$$\mu = \left(\frac{\alpha}{\pi f} \right)^{1/2} \quad (1)$$

where α is the thermal diffusivity of the sample, f is the modulation frequency of the incident radiation. In accordance with Eq. 1, a decrease in the modulation frequency causes an increase in thermal diffusion length. Therefore, the PA signal comes from a greater depth. Thus by altering the modulation frequency, depth profiling of the sample can be accomplished. Measurement of either the signal phase and/or the signal amplitude variation as a function of chopping frequency can lead to determination of the thermal diffusivity [24]. By determining its value, the thermal conductivity, K of the sample can be calculated.

Though the thermal property data of TiN coatings are important from the fundamental and technical point of view, very little work [25] has been done on measuring this quantity. In this article, we report the PA method for the measurement of thermal diffusivity and thermal conductivity of TiN thin films. The effect of microstructure, especially, grain size on the thermal property is investigated.

Experimental procedures

Sample preparation

TiN thin films were deposited on (111) oriented Si substrates by reactive DC magnetron sputtering. The TiN films were prepared by sputtering a 99.99% pure Ti disc of 3 in diameter and 2 mm thickness in a mixture of high purity argon (99.99%) and nitrogen (99.99%) plasma. The sputtering was carried out in a stainless steel chamber of 45 cm diameter and 20 cm depth using Mighty MAK, US sputtering gun of 3 in diameter. The silicon substrates used for the deposition of the films were of same dimension (10 mm \times 10 mm \times 0.5 mm) and were ultrasonically cleaned in acetone for 15 min and dried by blowing hot air before being placed in the vacuum chamber. Prior to deposition the system was flushed with argon alternately several times and, finally it was evacuated to a pressure of

1.2×10^{-5} mbar (1.2×10^{-3} Pa) by a turbo molecular pump coupled with a rotary pump. A halogen lamp (800 W, 6.3 A) heater, a chromel–alumel thermocouple and a digital temperature programmer/controller (LOGITEC, REPROC 3075) were used to maintain the substrates at the required temperatures. Series of TiN films were prepared at a substrate temperature of 973 K under different N_2 flow rates (2–30 standard cubic centimetre (sccm)) and at different substrate temperatures in the range 673–973 K under constant N_2 flow rate of 30 sccm. In all the cases, the argon gas flow rate was suitably adjusted to maintain the total flow rate of the gases at 40 sccm and the working pressure at 7.5×10^{-3} mbar (0.75 Pa). A 10 min pre-sputtering of the targets in pure argon with substrates shielded, was performed before each deposition process in order to sputter-etch the surface of the target and also to stabilize the sputtering condition. No bias voltage was applied to the substrates during sputtering. All the depositions were carried out for 60 min with a target to substrate working distance of 65 mm. The details of the deposition conditions are given in the Table 1.

The thickness of the deposited films was measured using a Sloan Dektak 6 M surface profilometer. The phase purity of the deposited films was confirmed in a Philips PW-1730 XRD system using Cu $K\alpha$ radiation. TiN films of thickness of about 10–20 nm deposited on sodium chloride substrates at 673 K and at 10 sccm of nitrogen flow rate were floated in distilled water and then picked up in Cu-grids. These samples were examined in a FEI Technai transmission electron microscope operating at 300 kV. The bulk values of density ($\rho = 5450 \text{ kg m}^{-3}$) and specific heat capacity ($C_v = 636 \text{ J kg}^{-1} \text{ K}^{-1}$) of TiN [26] were used in the calculation of the thermal conductivity of the TiN films.

Table 1 Sputtering parameters of TiN

Parameter	Conditions
Substrate	(111) Si single crystal, grounded
Substrate temperature	673–973 K
Distance between target and Substrate	6.5 cm
Base pressure	1.2×10^{-5} mbar (1.2×10^{-3} Pa)
N_2 flow rate	2–30 sccm
Ar flow rate	38–10 sccm
Total flow rate	40 sccm
Working pressure	7.5×10^{-3} mbar (0.75 Pa)
Target voltage	300–350 V
Plasma current	200 mA
Deposition time	60 min

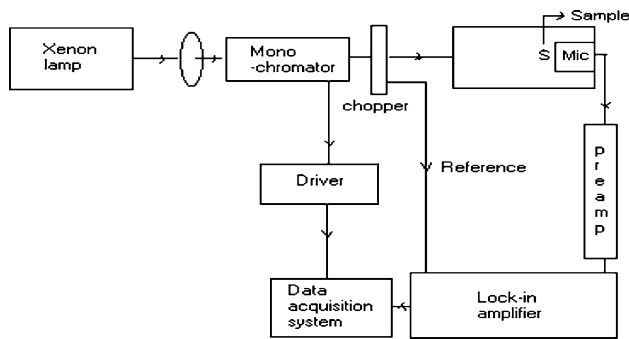


Fig. 1 Schematic diagram of an indigenously built photoacoustic spectrometer

Photoacoustic spectroscopy

A schematic diagram of the experimental setup used in the present study is shown in Fig. 1. Polychromatic light from a xenon lamp (400 W, Jobin Yvon) is mechanically chopped by a mechanical chopper (Model number PAR 650) and is focused onto the sample kept in an indigenously built sealed PA cell. A sensitive condenser microphone placed very close to the sample inside the PA cell detects the PA signal from the sample. The PA signal detected by the microphone is amplified using a single stage amplifier and the PA signal is finally detected by a lock-in-amplifier (Model Perkin Elmer 7225 DSP), which synchronizes the PA signal with a reference pulse from the chopper. The PA signal is influenced by the amount of heat generated in the sample and also on how the heat diffuses through the sample. Therefore, the technique offers a means to measure the thermal diffusivity (α) of the sample [27].

In order to determine the effective thermal diffusivity of the sample (substrate and thin films), the amplitude of the PA signal from the sample is recorded as a function of chopping frequency at room temperature. For an optically opaque and thermally thick sample ($\mu < 1$), the PA signal is given by

$$S = \frac{A}{f} \exp(-af^{1/2}) \quad (2)$$

where A is a constant that takes into account microphone characteristics and response time, temperature, incident radiation intensity and thermal properties of air, f is the modulation frequency of the incident light and a is the thermal diffusion coefficient of the material.

$$a = \left(\frac{\pi l^2}{\alpha} \right)^{1/2} \quad (3)$$

From a linear transformation of Eq. 2 and the slope of $\ln(fS)$ versus $f^{1/2}$ plot, the effective thermal diffusivity (α) of the sample, which includes contributions from TiN thin

film and silicon substrate is deduced. Knowing the effective thermal diffusivity, the thermal diffusivity of the constituent layers can be computed following two-layer model proposed by Mansanares et al. [28]. The effective thermal diffusivity (α) and the thermal diffusivities of the TiN thin film and silicon substrate are connected by the following equation [29]:

$$\frac{l}{\sqrt{\alpha}} = \frac{l_1}{\sqrt{\alpha_1}} + \frac{l_2}{\sqrt{\alpha_2}} \quad (4)$$

where l_1 , l_2 represent the thickness and α_1 , α_2 are the thermal diffusivities of substrate and TiN thin film, respectively. From this equation, the thermal diffusivity of TiN thin film is calculated knowing the thermal diffusivity value for Si. The thermal conductivity of TiN thin films is then calculated using the equation:

$$k = \alpha \rho C_v \quad (5)$$

where ρ is the density and C_v is the specific heat capacity of TiN.

Results and discussion

The as deposited TiN_x films exhibit metallic lustre and there is an apparent change in the colour of the films as a function of nitrogen flow rate. While the colour of the TiN_x films changes from brown at 2 sccm to golden yellow at 5 sccm and then to bronze yellow at flow rates ≥ 20 sccm. The scanning electron micrographs of the TiN films deposited under two different flow rates are shown in Fig. 2. The films are free of pores or cracks and show a featureless structure at increased nitrogen flow rates. The TiN films deposited at a nitrogen flow rate of 20 sccm and at 973 K exhibited an average hardness of 20 GPa by nano-indentation technique and the values are in agreement with the literature [30].

The XRD patterns of the TiN films deposited at constant temperature (973 K) and at different N_2 flow rates are shown in Fig. 3a. The films deposited at different temperatures and at constant N_2 flow rate of 30 sccm are shown in Fig. 3b. As the N_2 flow rate is increased from 2 to 5 sccm, the lattice parameter of TiN_x films also show an increase from 0.4211 to 0.4241 nm and beyond 5 sccm, it remains almost constant at 0.4245 nm. The initial increase in the lattice parameter of TiN_x films with increasing N_2 flow rate could be attributed to the transformation from substoichiometric TiN to stoichiometric TiN. Incorporation of nitrogen interstitially in the tetrahedral positions could result in the expansion of the titanium nitride lattice. The lattice parameter of TiN_x films deposited at 5 sccm is found to be close to the value of the bulk lattice parameter ($a = 0.424$ nm) and it possibly indicates the formation of

Fig. 2 Scanning electron micrographs of TiN films deposited at 973 K at different nitrogen flow rates: (a) 5 and (b) 20 sccm

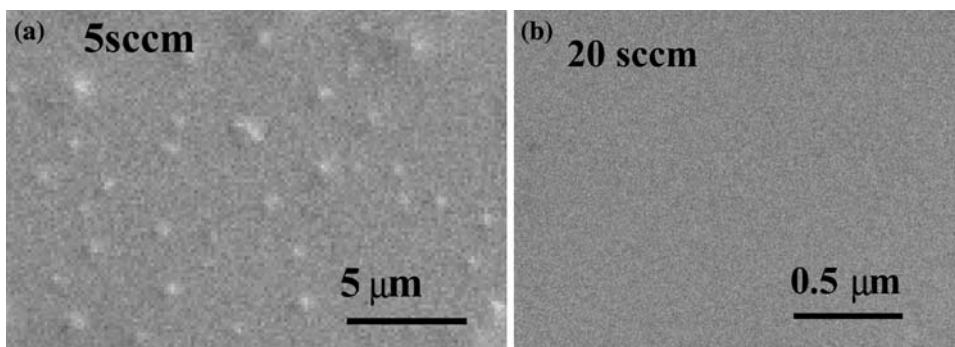
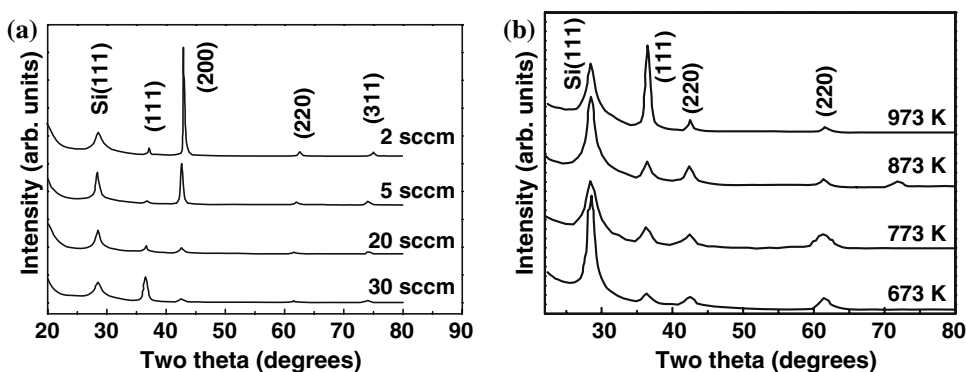


Fig. 3 XRD patterns of TiN thin films deposited at (a) different N₂ flow rates and at 973 K and (b) different temperatures and at 30 sccm of nitrogen



stoichiometric TiN_x. A slight increase in the lattice parameter of TiN_x beyond 5 sccm of N₂ flow rates could be due to the formation of hyperstoichiometric TiN_x.

Analysis of the XRD patterns shows that the films are single phasic δ-TiN and are polycrystalline in nature at ≥5 sccm. The large difference in the lattice parameter of TiN (~0.424 nm) and Si (~0.543 nm) produces a lattice mismatch of about 21.9% and it could possibly promote the formation of polycrystalline films of TiN. However, it is noticed that at 973 K, (111) orientation is more dominant than that of the normally observed (200) orientation (Fig. 3b). This change in the orientation of the film, in general, is controlled by interfacial stresses due to the lattice mismatch of the film with the substrate and is strongly influenced by the substrate temperature and deposition rate [31]. For a constant deposition rate, there exists a critical temperature above which a preferred orientation or epitaxy is facilitated [32]. Though (200) reflection represents 100% intensity line for TiN for the powder XRD pattern reported in JCPDS, the formation of (111) orientation significantly reduces the lattice mismatch with Si (111) from 32% to 22% because of the increased supply of thermal energy at 973 K. These factors promote the (111) preferred orientation of TiN at 973 K.

The relative grain size of the films was calculated from the full width at half maximum (FWHM) of the (200) peak using Scherrer’s equation, $D = 0.9\lambda/(\beta \cos \theta)$; where D is the average grain size, λ is the wavelength of the X-rays

used, β is the FWHM (in radians) and θ is the diffraction angle. However, the measured FWHM by Gaussian peak fitting procedure did not include the effects of instrumental broadening and strain in the films. It is found that the grain size of the films decreases from 36 to 10 nm as the N₂ flow rate is increased from 2 to 30 sccm (Table 2) and increases from 7 to 10 nm as the substrate temperature is increased from 673 to 973 K (Table 3). The influence of nitrogen flow rate on the grain size is found to be more significant than that of the substrate temperature. TEM examination of plan view samples of TiN films showed nanocrystalline grains of size of about 10 nm (Fig. 4) and the corresponding diffraction pattern is shown in the inset of figure. The spotty diffraction patterns correspond to (111), (200), and (220) reflections and qualitatively indicate the preferred orientation of the grains. A similar microstructural feature was observed on TiN films grown at room

Table 2 Grain size, thermal diffusivity and thermal conductivity of TiN films deposited at 973 K and at different N₂ flow rates

N ₂ flow rate (sccm)	Grain size (nm)	Thermal diffusivity ($\times 10^{-7} \text{ m}^2 \text{ s}^{-1}$)	Thermal conductivity ($\text{W m}^{-1} \text{ K}^{-1}$)
2	36.60	8.568	2.97
5	22.47	8.193	2.84
20	14.00	7.963	2.76
30	10.00	7.856	2.72

Table 3 Grain size, thermal diffusivity and thermal conductivity of TiN films deposited at different substrate temperatures and at a N₂ flow rate of 30 sccm

Temperature (K)	Grain size (nm)	Thermal diffusivity ($\times 10^{-7} \text{ m}^2 \text{ s}^{-1}$)	Thermal conductivity ($\text{W m}^{-1} \text{ K}^{-1}$)
673	7.20	7.761	2.69
773	7.35	7.764	2.69
873	9.00	7.818	2.71
973	10.00	7.856	2.72

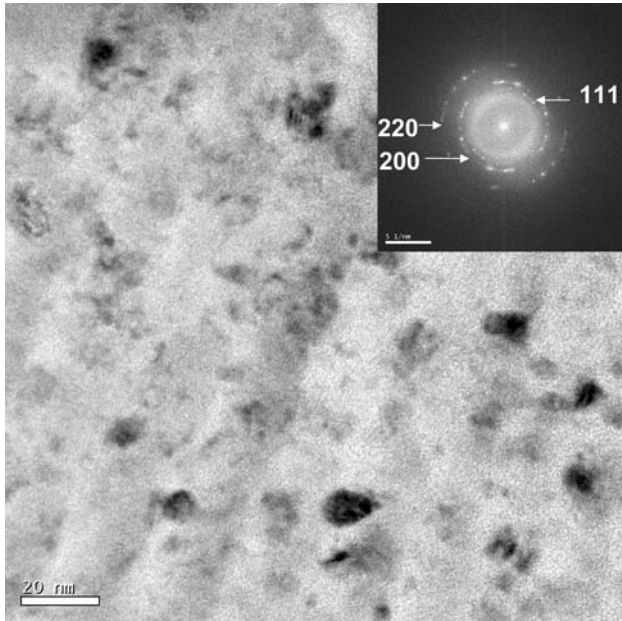


Fig. 4 TEM bright field image of the TiN thin film deposited at 673 K showing nanocrystalline grains and the inset shows the diffraction pattern of the film

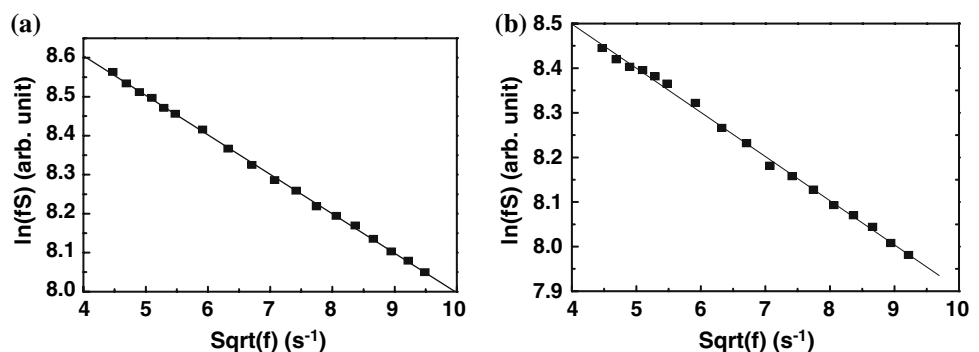
temperature by radio-frequency sputtering [33]. It was shown that the films contain nanocrystals of size 5–10 nm. Since the films were grown in the temperature range

673–873 K, it is believed that the amount of amorphous content could be very low in the present investigation.

As discussed in “Photoacoustic spectroscopy” section, the thermal diffusivity of the films was determined using PA method. The plots between $\ln(fS)$ and $f^{1/2}$ were drawn for the films deposited at different flow rates and substrate temperature. Typical examples of the plots for the films deposited at 973 K and at N₂ flow rate of 5 sccm and for the films deposited at 673 K at N₂ flow rate of 30 sccm are shown in Fig. 5a and b, respectively. The value of thermal diffusivity and thermal conductivity of TiN films obtained by PA method are given in Tables 2 and 3. The error involved in measurement of thermal diffusivity is $\pm 2\%$.

It is well known that the thermal conductivity of thin films may differ significantly from the bulk value due to the difference in the microstructural features such as grain size, amorphousness, concentration of foreign atoms, and defects which strongly affect the scattering process of energy carriers [20]. Scattering of phonons occurs when they interact with lattice imperfections, which include vacancies, dislocations, grain boundaries, atoms of different masses and other phonons. Of these the grain boundary scattering has least effect in conventional materials, but may provide a significant effect in nanostructured coatings, particularly when the grain size is of the same order as the mean free path for phonon scattering [34]. From Tables 2 and 3, it is noticed that the thermal conductivity of all the TiN thin films is found to be one order of magnitude less than the bulk value of 30 W/mK [25]. There are many reports in the literature where the thermal conductivity of thin films is found to be less than the bulk by one order or more [25, 35–38]. Based on theoretical calculations, Popov et al. [35] have shown that the thermal conductivity of a film is considerably lower than that of bulk structure. Calculations of Kabacoff [36] on the influence of nano-grain size on the phonon conductivity of zirconia-7 wt% yttria coatings as a function of temperature have shown that the thermal conductivity is drastically reduced for fine-grained materials particularly when the grain size is of

Fig. 5 Depth profile analysis of TiN thin films deposited at (a) 973 K, 5 sccm and (b) 673 K, 30 sccm



nanometer dimensions. Bodzenta et al. [37] measured the thermal properties of AlN, AlN–GaN films deposited on Si and GaAs substrates by photothermal measuring methods based on thermal wave propagation in a layered structure in 3D geometry and found that the values are three to four orders smaller than that of the bulk materials. Jacquet et al. [38] have shown that the thermal conductivity of the AlN thin films is strongly reduced compared to the bulk, for example, the reduction is about three orders of magnitude at 100 K by cross-plane thermal conductivity measurements. Rhode [25] has performed PA measurements of thermal conductivity of sputtered films of Au, TiN, Al₂O₃ and electroplated films of Ni on different substrates using Ar ion laser and found that the thermal conductivity of the films is strongly reduced compared with the bulk values. It was further reported that the thermal conductivity of TiN films of 5 μm thick on Si substrates with different adhesion strengths were in the range 3.3–3.8 W/mK, and these are in close agreement with our values.

In the present study, the grain size of the TiN films deposited at constant substrate temperature and at different N₂ flow rates decreases with increasing N₂ flow rates. The corresponding thermal diffusivity and thermal conductivity of TiN films also decrease with increasing N₂ flow rate. In contrast, the grain size of the TiN films deposited under a constant N₂ flow rate and at different substrate temperatures increases with increasing temperature and the corresponding values of thermal diffusivity and thermal conductivity of the films increase slightly with increasing temperature. Thus, the results clearly demonstrate that the grain size of the thin films has substantial influence on the thermal properties of TiN thin films.

Scattering mechanisms due to grain boundaries seem to contribute significantly to the variation of the thermal conductivity of TiN thin films. Increased grain sizes are noticed at higher substrate temperatures or at low nitrogen flow rates. At low substrate temperature, the nucleation frequencies are higher and the growth rates are lower. As the substrate temperature increases, there is an increase in the adatom mobility of the sputtered species on the substrate. This causes an increasing grain size with increasing substrate temperature. On the other hand, when the N₂ flow rate is increased, there could be significant distortions in the TiN lattice due to incorporation of excess nitrogen atoms at the interstitial positions of the lattice. The Ti–N system seems to tolerate the distortions by reducing the grain size. When the lattice is distorted from its regular structure, there is a possibility of increased phonon scattering [39]. Accommodation of excess nitrogen atoms at the interstitial positions would generate local strain fields and these strain fields would scatter phonons directly, thus increasing the phonon dispersion in the lattice. With the increased dispersion, there is an enhanced probability of

phonon–phonon interactions that would further reduce the phonon mean free path. Also when the grain size decreases, the grain boundary area increases and hence the probability of phonon scattering significantly increases. All these lead to the enhanced phonon scattering resulting in reduced mean free path of the phonons. It is known that when the phonon mean free path decreases the thermal conductivity decreases, since $k = \frac{1}{3}C_v v l$, where C_v is the specific heat capacity of TiN, v is the velocity of phonons and l is the mean free path of the phonons. On the other hand, with the increasing substrate temperature, the grain size of the films increases. When the grain size of the films increases the grain boundary area decreases and hence the probability of phonon-internal grain boundaries scattering decreases resulting in the increased mean free path of phonons leading to an increase in the thermal conductivity of the films. These observations are in line with the literature [34, 38].

Measurement of thermal property as indicated earlier would be of great advantage for enhancing the life time of components. The PA technique as a non-destructive tool provides a method to measure thermal properties of the films and it could also be used to correlate the thermal properties with the microstructure of the films. Though in the present study, the grain size seems to have a greater effect on the thermal conductivity of the films, one cannot ignore the role of other factors like defect concentration, surface morphology and thickness, and the effect of the latter factors will be reported in our future work.

Conclusions

The thermal properties of the TiN films deposited by reactive DC sputtering have been studied by PA method. Following are the important conclusions drawn from the present study.

- (i) The thermal conductivity of TiN thin films is found to be one order of magnitude less than the corresponding bulk value, which has been mainly attributed to nanocrystalline grains.
- (ii) The thermal conductivity of the films increases with the decreasing N₂ flow rates and decreases with decreasing substrate temperature, which could be explained on the basis of the variation in grain size, and its influence on the phonon scattering.

Acknowledgements The authors would like to thank Dr. M. Vijayalakshmi, Head, Physical Metallurgy Division, Dr. P.R. Vasudeva Rao, Director of Metallurgy and Materials Group and Dr. Baldev Raj, Director, IGCAR, Kalpakkam. One of the authors (A. Albert Iru-dayaraj) gratefully acknowledges the support and encouragement

given by UGC, Vellore Institute of Technology, Vellore and Sacred Heart College, Tirupattur.

References

1. Banerjee R, Chandra R, Ayyub P (2002) *Thin Solid Film* 405:64
2. Valvoda V (1995) *J Alloy Compd* 219:83
3. Ting CY (1982) *J Vac Sci Technol* 21(1):14
4. Kim NY, Son JB, Oh JH, Hwangbo CK, Park MC (2000) *Surf Coat Technol* 128–129:156
5. Vaz F, Machado P, Rebouta L, Cerqueira P, Goudeau Ph, Riviere JP, Alves E, Pischow K, de Rijk J (2003) *Surf Coat Technol* 174–175:375
6. Patsalas P, Charitidis C, Logothetidis S (2000) *Surf Coat Technol* 125:335
7. Armigliato A, Celotti G, Garulli A, Guerri S, Ostoja P, Rosa R (1982) *Thin Solid Film* 92:341
8. Pelleg J, Zevin LZ, Lungo S, Croitoru N (1991) *Thin Solid Film* 197:117
9. Asinovsky L, Frisa LE (1998) *Thin Solid Film* 313–314:303
10. Ellwanger RC, Towner JM (1988) *Thin Solid Film* 161:289
11. Sundgren JE (1985) *Thin Solid Film* 128:21
12. Yu G, Chen J, Shi Y, Pan HC, Zhu D, Xu H, Zheng Z (1998) *Thin Solid Film* 335:59
13. Ma LW, Cairney JM, Hoffman M, Munroe PR (2005) *Surf Coat Technol* 192:11
14. Volkelein F (1990) *Thin Solid Film* 188:27
15. Cahill DG, Alleu TH (1994) *Appl Phys Lett* 65:309
16. Okuda M, Ohkuba S (1992) *Thin Solid Film* 213:176
17. Goodson KE, Flik MI, Su LT, Antoniadis DA (1994) *ASME J Heat Transfer* 116:317
18. Goodson KE, Kading OW, Rosler M, Zachai R (1995) *J Appl Phys* 77:1385
19. Wu ZL, Reichling M, Hu XQ, Balasubramanian K, Guenther KH (1993) *Appl Opt* 32:5660
20. Wang X, Hu H, Xu X (2001) *ASME J Heat Transfer* 123:138
21. Pandhija S, Rai N, Singh AK, Rai AK, Gopal R (2006) *Progr Cryst Growth Character Mater* 52:53
22. Raji P, Sanjeeviraja C, Ramachandran K (2004) *Cryst Res Technol* 39(7):617
23. Pichler A, Sowa MG. (2005) *J Mol Spectrosc* 229:231
24. Lachine A, Poulet P (1984) *Appl Phys Lett* 45(9):953
25. Rohde M (1994) *Thin Solid Films* 238:199
26. <http://www.freepatentsonline.com>. Accessed on 20 June 2007
27. Anjos V, Bell MJV, de Vasconcelos EA, da Silva Jr EF, Andrade AA, Franco RWA, Castro MPP, Esquef IA, Faria Jr RT (2005) *Microelectr J* 36:977
28. Mansanares AM, Bento AC, Vargas H, Leite NF, Miranda LCM (1990) *Phys Rev B* 42:4447
29. Tominaga T, Ito K (1988) *Jpn J Appl Phys* 27(2):392
30. Ma CH, Huang JH, Chen H (2006) *Surf Coat Technol* 200:3868
31. Singh RK, Biunno N, Narayan J (1989) *J Appl Phys* 65:2398
32. Sloope BW, Tiller CO (1965) *J Appl Phys* 36:3174
33. Kim T-S, Park S-S, Lee B-T (2005) *Mater Lett* 59:3929
34. Nicholls JR, Lawson KJ, Johnstone A, Rickerby DS (2002) *Surf Coat Technol* 151–152:383
35. Popov D, Jacimovski SK, Tosic BS, Setrajcic JP (2003) *Physica A* 317:129
36. Kabacoff LT (1998) Thermally sprayed nano-structured thermal barrier Coatings, NATO Workshop on Thermal barrier Coatings, Aalborg, Denmark, AGARD-R-823, Paper 12
37. Bodzenta J, Burak B, Jagoda A, Stanczyk B (2005) *Diamond Relat Mater* 14:1169
38. Jacquot A, Lenoir B, Dauscher A, Verardi P, Cracium F, Stolzer M, Gartner M, Dinescu M (2002) *Appl Surf Sci* 186:507
39. Padture NP, Klemens PG (1997) *J Am Ceram Soc* 80(4):1018